International Journal of Heat and Mass Transfer 160 (2020) 120230

Contents lists available at ScienceDirect

International Journal of Heat and Mass Transfer

journal homepage: www.elsevier.com/locate/hmt

Experimental study on single-phase hybrid microchannel cooling using HFE-7100 for liquid-cooled chips

Min Yang[a], Mo-Tong Li[a], Yu-Chao Hua[a], Wei Wang[b,*], Bing-Yang Cao[a,*]

[a] Key Laboratory for Thermal Science and Power Engineering of Ministry of Education, Department of Engineering Mechanics, Tsinghua University, Beijing, 100084, China

[b] National Key Laboratory of Science and Technology on Micro/Nano Fabrication, Frontiers Science Center for Nano-optoelectronics, Institute of Microelectronics, Peking University, Beijing, 100871, China

ARTICLE INFO

Article history:
Received 27 March 2020
Revised 21 June 2020
Accepted 20 July 2020

Key words:
Microchannel heat sink
Hybrid design
Manifold concept
Secondary channels
Single-phase cooling experiment
Hydraulic and thermal performance enhancements

ABSTRACT

It is highly desired to efficiently dissipate the high heat flux generated in electronics. A novel hybrid microchannel heat sink combining manifold with secondary oblique channels (MMC-SOC) has been proposed and studied numerically in our previous work. The current study conducts the fabrication and experimental test of the hybrid microchannel heat sink using dielectric fluid HFE-7100. The volume flow rate q_v ranges from 211 to 580 mL/min, with channel Reynolds numbers between 278 and 905 for heat fluxes q'' = 20, 25, 30 and 35 W/cm^2. The results indicate that the MMC-SOC heat sink can simultaneously reduce the thermal resistance R_t and pressure drop ΔP. For heat sinks with channel height H_c = 60 μm, an 11% reduction in ΔP and a 24% reduction in R_t are obtained compared to conventional manifold microchannel (MMC) heat sink for q_v = 580 mL/min and q'' = 20 W/cm^2. As q_v increases, the ratio (R_t/R_{t0}) becomes smaller and $(\Delta P/\Delta P_0)$ becomes larger, which indicates an enhanced ability of reducing R_t and a suppressed ability of reducing ΔP. For the maximum q_v = 580 mL/min and q'' = 35 W/cm^2, the MMC-SOC heat sink can maintain a maximum chip temperature of 53 °C with a pressure drop of only 3.77 kPa. Moreover, the proposed MMC-SOC heat sink has a lower pressure drop compared to MMC heat sink owing to a reasonable design, even though the Reynolds number of the MMC-SOC heat sink reaches up to 883. This provides a very promising scheme for safe and efficient single-phase microchannel cooling used in the thermal management of electronics with high heat flux. In addition, the ratio (R_t/R_{t0}) will increase with increasing heat flux and increasing the flow rate becomes an effective way to further reduce the chip surface temperature at operating conditions with higher heat flux.

1. Introduction

With the rapid development of fabrication and packaging technologies, the incorporated transistors in a chip increase sharply [1-3]. The packaging density is further increased by the 3D integrated circuit packaging technology [4,5]. Consequently, the heat flux in various electronic devices keeps increasing, which requires efficient cooling technologies to ensure the safety and lifetime of electronics [6-9]. Thermal management has become an essential issue that should be considered for further integration and miniaturization of electronics [10-12]. Compared to air cooling, liquid cooling strategy [13-16] is becoming increasingly important to electronic devices with high heat flux because of a relatively high thermal conductivity of liquid. A number of liquid cooling schemes have been introduced in literature, such as jet-impingement [17-19], spray cooling [20-22], microchannel cooling and micro pin-fin array cooling schemes [23-25]. Among these cooling schemes, microchannel cooling has attracted more attention due to its high heat removal capability and high reliability [26,27]. After Tuckerman and Pease firstly proposed microchannel heat sink in 1981 [23], it has become one of the most promising technologies to solve those thermal management problems encountered in various electronics with high power density. Encouraged by Tuckerman and Pease, numerous works have been conducted to identify the thermal and pressure-drop characteristics of microchannel heat sink in early studies [28-31]. However, microchannel cooling has two distinct disadvantages. On the one hand, a nonuniform temperature distribution can be observed at heat source due to the continuous heat absorption along the flow direction. Another problem is that exor-

* Corresponding author.
E-mail addresses: w.wang@pku.edu.cn (W. Wang), caoby@tsinghua.edu.cn (B.-Y. Cao).

https://doi.org/10.1016/j.ijheatmasstransfer.2020.120230
0017-9310/

Nomenclature

d	secondary channel width (m)
D_h	hydraulic diameter (m)
f	Darcy friction factor
H_c	channel height (m)
I	electrical current (A)
k	thermal conductivity (W/m K)
L	flow length (m)
P_p	pumping power (W)
ΔP	pressure drop (Pa)
q''	heat flux (W/m^2)
Q	total heat flux (W)
q_v	volume flow rate (m^3/s)
R	thermal resistance (K/W)
Re	Reynolds number
T	Temperature (K)
u	flow velocity (m/s)
U	electrical voltage (V)
W_c	channel width (m)
W_w	channel space (m)
W_{in}	manifold inlet width (m)
W_{out}	manifold outlet width (m)

Subscripts

0	original design
ave	average
c	channel
in	inlet
t	total
out	outlet
w	wall

Greek symbols

ρ	density (kg/m^3)
μ	dynamic viscosity (kg/(m s))

bitant pressure drop is required for high heat removal, which gives rise to a considerable challenge to design and manufacturing of the driven pump. Therefore, extensive research has been implemented to reduce the pressure loss and temperature of microchannel heat sink, such as fractal microchannel [32,33], microchannel heat sink with wavy channel [34,35], double-layer microchannel heat sink [36-38], manifold microchannel heat sink [39-46] and secondary flow [47-50]. These strategies can increase the effective heat transfer area and enhance fluid disturbance, i.e. optimization of the synergy degree between velocity and temperature fields [51]. Of these cooling strategies, secondary flow and liquid distribution manifold are considered as the two most effective solutions. A manifold microchannel (MMC) heat sink utilizes alternate inlet and outlet conduits formed by the liquid distribution manifold, resulting in a significant reduction in flow length and the corresponding pressure drop. Moreover, the manifold structure can produce heat transfer enhancement like jet-impingement. Extensive research has been done on the thermal-fluidic performance of manifold heat sink [39-46]. Another effective technique to enhance the heat transfer is secondary flow. Offset strip fins located in the substrate can form many smaller cooling liquid channels, i.e. secondary channels. It can generate secondary flow, which can enhance heat transfer by generating vortex and thinning the boundary layer. Secondary channels can also enlarge the convection surface area and bring higher cooling capability. However, as pointed by Steinke et.al [47], the extra pressure drop caused by secondary flow is the limiting factor if the geometric parameters are not designed properly. In addition, the dielectric liquid is an ideal coolant compared to water considering its low risk [43].

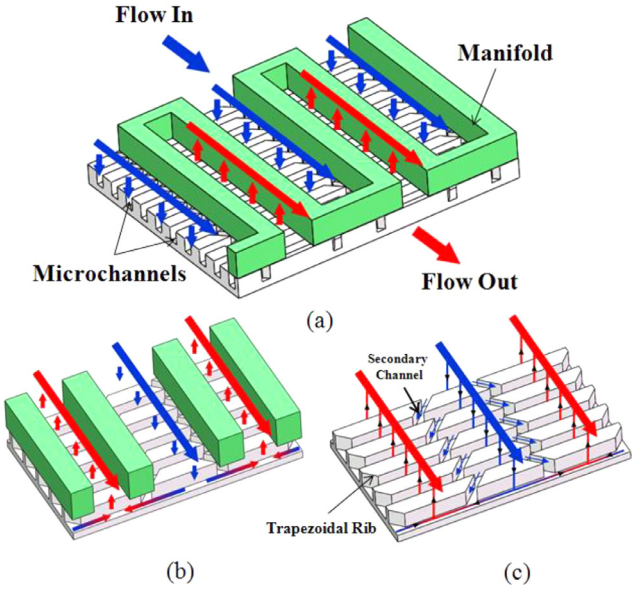

Fig. 1. A schematic diagram of the hybrid microchannel heat sink: (a) 3D view, and cross-sectional views of the heat sink (b) with manifold, (c) without manifold.

Although performance enhancement can be obtained through manifold structure or secondary flow, single enhancement scheme can no longer meet the rapid growth of heat generation with the continuous increasing power density in various electronic components, which is expected to be more than 1 kW/cm^2 in the near future [52]. Therefore, combining benefits of various performance enhancement schemes is of critical importance for future electronic components. Recently, we have proposed a novel hybrid cooling scheme combining manifold architecture with secondary oblique channels [53]. The aim of the hybrid cooling scheme is to reduce both temperature and pressure loss. A schematic of the hybrid MMC-SOC heat sink is described in Fig. 1. On the top side of the silicon microchannel plate is the coolant distribution manifold layer used as the liquid-feeding system (Fig. 1(a)). The silicon microchannel plate contains 34 parallel microchannels, as well as one resistance heater and three temperature sensors, as presented later. It should be noted that the cold coolant will move into the microchannels by a turn angle of 90 when it flows along the individual inlet channels, which is capable of cooling the heat source in a way of direct impinging jet. Subsequently, coolant within each microchannel will travel in opposite directions and then leave the microchannel, finally flow back to the outlet channel formed by the manifold structure. In order to visually illustrate the flow paths in the hybrid heat sink, the isometric section views with and without manifold distributor are presented in Figs. 1(b) and (c). It is obvious that the manifold system allows the flow length in each microchannel and the corresponding pressure loss to be reduced significantly. In addition, the traditional straight fin is broken into trapezoidal ribs to form discontinuous secondary channels. Therefore, when the coolant flows along the main microchannel, some of it will also enter into the secondary channel, which can enhance the flow mixing.

Our previous numerical simulations [53] have indicated that the MMC-SOC heat sink could reduce the pressure loss and heat source temperature simultaneously compared to MMC heat sink. The current study aims to verify the superiority of the proposed hybrid heat sink by single-phase cooling experiments. In the current experimental study, we design and fabricate the hybrid mi-

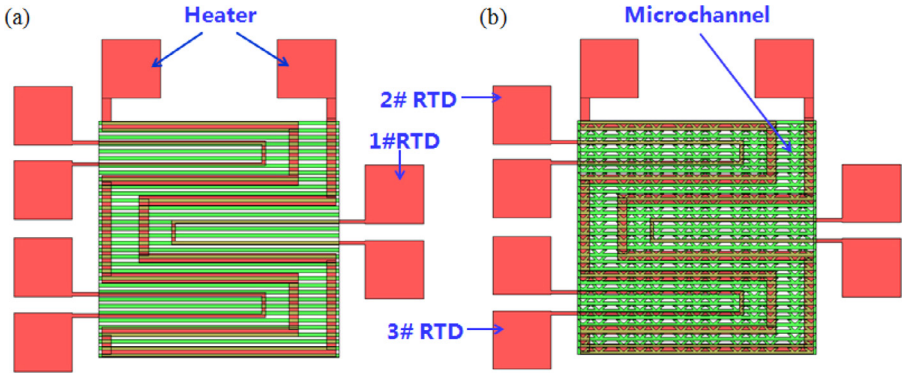

Fig. 2. Schematic design of the test device: (a) straight microchannel, (b) microchannel with secondary channels.

crochannel heat sink and traditional manifold mircochannel heat sink according to our previous work [53]. Their single-phase hydraulic and thermal performances are measured experimentally. HFE-7100 is used as the working fluid and fluid flow rates between 211 mL/min and 580 mL/min are tested with applied heat fluxes of 20–35 W/cm^2. The experimental results indicate that the MMC-SOC heat sink has superior overall performance compared to conventional MMC heat sink.

2. Test module design and fabrication

2.1. Microchannel plate fabrication

In the current study, two types of microchannels are fabricated and tested experimentally, with the layouts shown in Fig. 2, i.e. (a) straight microchannel and (b) microchannel with secondary channels. A Cr/Pt/Au serpentine heater covering a 1 × 1 cm^2 area is designed on one side of the silicon substrate to provide uniform heating. In addition, three resistance temperature detectors (RTDs) are placed between the heater lines used for temperature measurement. It should be noted that those three RTDs are respectively located at the upper, the middle and the lower places of the chip to provide a relatively clear picture of the chip temperature. On the other side of the substrate, 34 parallel microchannels or microchannels with secondary channels are designed within the heating area. The width and overall length of the microchannel are 150 μm and 10 mm, respectively. The fabrication process is briefly illustrated in Fig. 3, starting from a double-polished wafer with thickness of 400 μm. A SiO_2 layer of 300 nm thick was firstly thermally grown on Si substrate for the electrical insulation for the heater and temperature sensors. Moreover, the oxide also functioned as the etching mask for deep microchannels fabrication. As indicated in Figs. 3(a)-(c), the serpentine platinum heater and sensors were prepared by a lift-off process using a positive photoresist (PR) (RZJ-304 (25), Suzhou Ruihong Co., Suzhou, China) as the sacrificial layer. A 20-nm-thick Cr layer, 200-nm-thick Pt layer and 50-nm-thick Au layer were deposited sequentially using sputtering technique. The thin Cr film was used to ensure a good adhesion between the platinum film and the oxide layer, while the Au was used to facilitate the subsequent soldering process between the test chip pads and the printed circuit board (PCB). Fig. 4(a) shows the fabricated serpentine heater and RTDs. The thermal test chip has a size of 2 × 2 cm^2, and the center heating area is 1 × 1 cm^2. It should be noted that a layer of photoresist was deposited on the pattern to prevent any damage caused by the subsequent microchannel fabrication. In addition, in order to connect the test chip with a closed-loop flow system, a custom printed circuit board was designed and fabricated, as shown in Fig. 4(b).

Microchannels were then patterned on the other side of the silicon substrate (Figs. 3(d)-(f)), matching the heater and sensors. Deep reactive ion etching (DRIE) was applied to etch the silicon and the stripping of PR-layer was then conducted. It should be pointed out that the deviation of DRIE is less than 0.5% and the microchannel area is only 1 × 1 cm^2, which can ensure channel height good uniformity. Buffered oxide etching (BOE) was used to remove the remaining SiO_2 layer on the microchannel side. Fig. 5 is the scanning electron microscope (SEM) images of the fabricated microchannels. The overall size of the microchannel area is 1 × 1 cm^2. The widths of the channel W_c and the channel space W_w are both 150 μm. The longer side of the trapezoid fins appearing under the manifold inlet channel is W_1 = 700 μm, twice as long as that of the trapezoid fins W_2 appearing at other place. The width d between two trapezoid fins is 150 μm. The acute angle of those trapezoid fins is 45° Two channel heights, H_c = 60 μm and 100 μm, are designed for comparative studies. MMC-1 or MMC-SOC-1 represents heat sink with H_c = 60 μm and MMC-2 or MMC-SOC-2 represents heat sink with H_c = 100 μm. Those critical measured geometric values are measured and summarized in Table 1. D_h is the channel hydraulic diameter and is defined as:

$$Dh = \frac{2WcHc}{Wc + Hc}. \quad (1)$$

2.2. Manifold fabrication

Fig. 6 presents the 3D-printed (Projet MJP 2500 plus, 3D systems, Rock Hill, SC, USA) manifold structure for flow distribution application using VisiJet CR-WT. The inlet and outlet tubes used to guide the coolant to flow into and out of the test module are located at opposite sides of the structure. There are two thermometer holes located near the inlet and outlet tubes and two T-type thermocouples were inserted into the holes to measure the inlet and outlet coolant temperatures. The distribution manifold is located at the center of the structure and half of it is shown in Fig. 6(b). Four inlet and five outlet channels are formed to split a cold liquid stream from the inlet tube and then combine the coolant into a stream to the outlet tube. In addition, guided by the distribution manifold, coolant is able to impinge on the heat source and further reduce the chip temperature. The widths of in-

Table 1
Summary of microchannel test sample dimensions in this study.

Sample	W_c (μm)	W_w (μm)	H_c (μm)	D_h (μm)
MMC-1	148.6	147.2	61.5	87.0
MMC-2	151.1	149.3	103.2	122.6
MMCSOC-1	149.5	153.7	59.3	84.9
MMCSOC-2	150.1	146.3	103.5	122.5

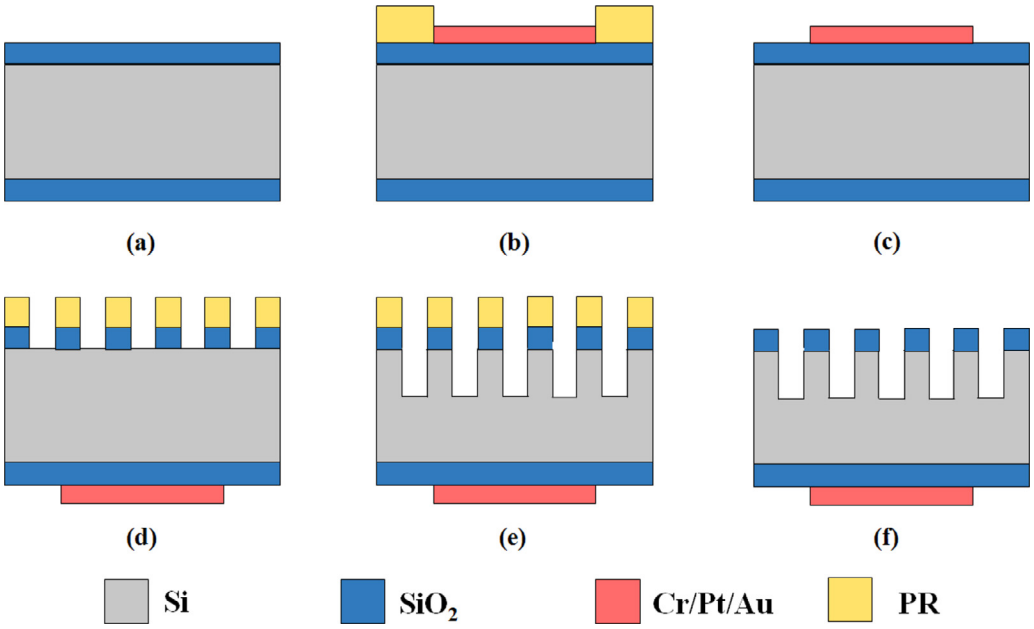

Fig. 3. Schematic of the microchannel heat sink fabrication: (a) thermally grow oxide layers on the double-polished silicon substrate; (b) define the heater and RTDs by a lithography process and then deposit Cr/Pt/Au layers on the cold plate by sputtering technique; (c) lift-off process; (d) define microchannels by a lithography process and then dry-etch into the oxide layer; (e) deep reactive ion etching (DRIE) of the silicon; (f) strip PR and remove the remaining oxide layer at the channel side.

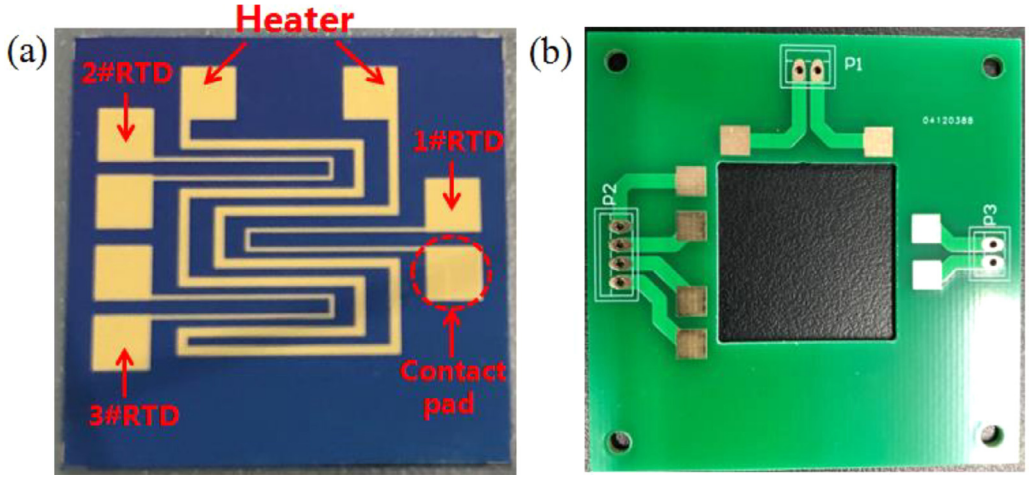

Fig. 4. Photographs of (a) the serpentine heater, RTDs, and contact pads on the test chip; (b) the custom printed circuit board.

let channel W_{in} and outlet channel W_{out} are 700 μm and 350 μm, respectively. In addition, two positioning structures are designed near the inlet tube to guide the adhesive between the chip and manifold structure.

2.3. Test module assembly

The final assembly of the test module is mainly divided into two steps: Firstly, 770 silicone surface treatment agent and 406 instant adhesive were used to brush the working surfaces of silicon and manifold. Then the two surfaces were stuck together through the instant adhesive 406. The adhesive was aligned with the manifold using two positioning structures. It should be noted that the above operations can avoid any adhesive overflowing the required area. Secondly, soldering process was carried out to connect the test chip with PCB by copper wire. Fig. 7 shows the test module of microchannel heat sink in the current study. It contains a 3D-printed polycarbonate manifold structure, microchannel plate and printed circuit board. The manifold structure was mounted under the test chip. As described in previous section, the size of the test chip is 2 $\times$ 2 cm^2 with the center 1 $\times$ 1 cm^2 heating area. There are three RTDs and a resistive heater located at the heating area, which can independently control the local temperature measuring and heating. A DC power supply (N5752A, Keysight) was connected to the PCB to provide the input power.

3. Experimental methods

3.1. RTD calibration

Prior to the experiment, the calibration process of RTDs was performed in a vacuum oven by varying the temperature and recording corresponding electrical resistance for individual RTDs. The temperature was in the range of 30 °C to 100 °C, in steps of 5 °C. A unique voltage-temperature response was developed for each of the three sensors. The measured temperature coefficients of resistance (TCR) of RTDs were 1.443 $\times$ 10^{-3}, 1.454 $\times$ 10^{-3} and

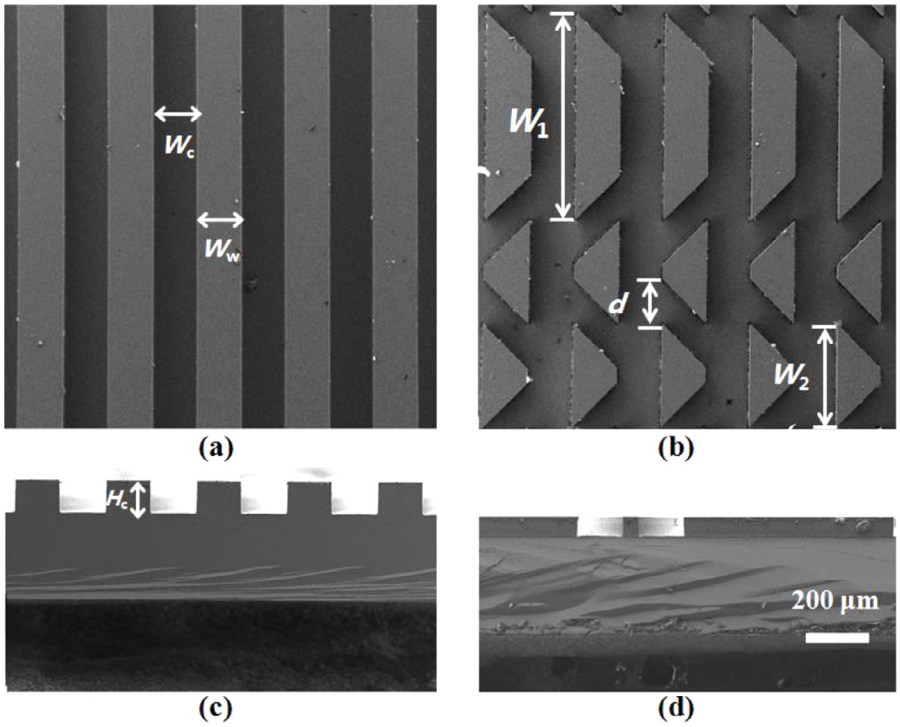

Fig. 5. SEM images of heat sink (a) straight microchannel, (b) microchannel with secondary channels, (c) (d) are channel cross-sections.

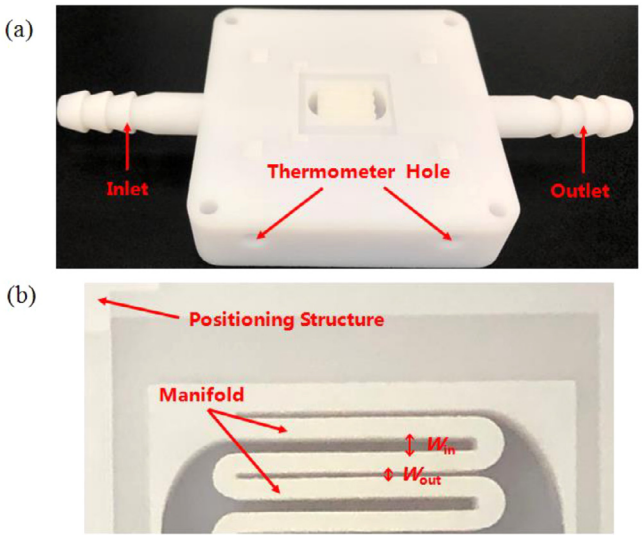

Fig. 6. (a) 3-D printed manifold structure used for microchannel heat sink, (b) half of the distribution manifold.

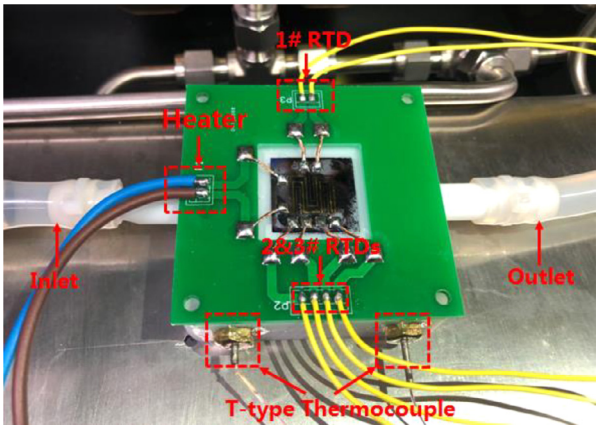

Fig. 7. Microchannel test module.

$1.472 \times 10^{-3}\ °C^{-1}$, respectively. The calculated maximum uncertainty for RTD was about ±0.23 °C.

3.2. Flow loop

The flow loop used to provide coolant for the test chip is shown in Fig. 8. The coolant is driven by a gear pump (GB-P23, Micropump) from a liquid reservoir into the test module. A Coriolis mass flow meter (DMF-1–1B, Beijing Sincerity Automatic Equipment Co., Ltd) is used to measure the liquid mass flow rate. HFE-7100 (3 M Co., USA) stored in the liquid reservoir is used as the working fluid for its low risk compared to water. Pressure transducer (STG 74S, Honeywell) and pressure drop transducer (STD735, Honeywell) are respectively used to measure the inlet gage pressure and the pressure loss ΔP between the inlet and outlet of the test module. The inlet T_{in} and exit T_{out} coolant temperature measurements are conducted by two T-type thermocouples inserted into the manifold structure. The inlet fluid temperature is maintained in the range of 20±0.5 °C by a thermal bath. Another thermal bath is prepared to cool the exiting coolant from the test module before it returns to the reservoir. Liquid is carefully cleaned by a 20 μm filter placed before the pump. Moreover, a 40 μm filter is used to prevent channel blockage before the test module. A multi-channel data acquisition system (34972A, Keysight) is applied to collect various data, including temperatures, inlet pressure, pressure drop, mass flow rate. During the experiment, tubes used for liquid transportation are wrapped in an insulating shroud. In addition, a 3D-printed plastic cover plate is placed on the test module to minimize the heat loss. The maximum heat loss to the ambient can be obtained when the heat flux is 35 W/cm^2 and it is less than 6% of the total heat input. Thus, the heat loss can be assumed to be negligible.

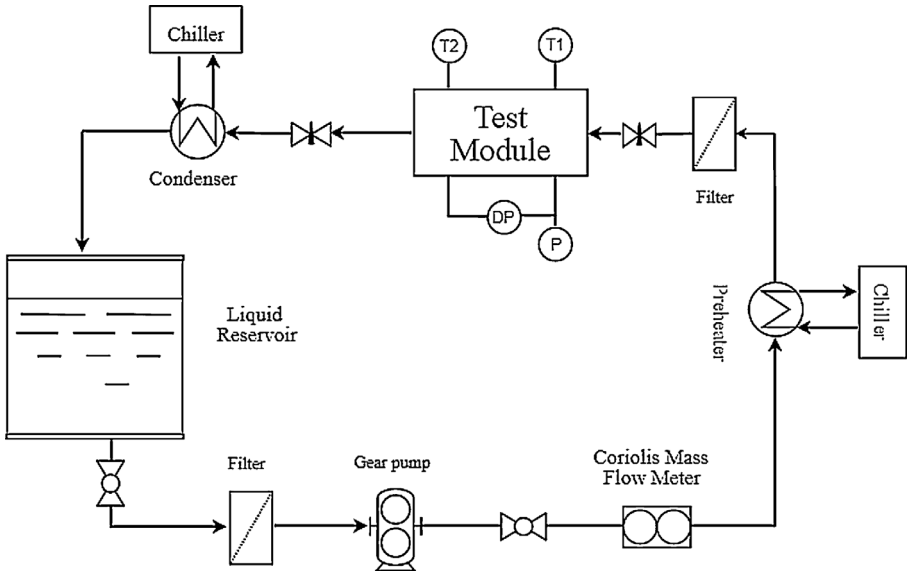

Fig. 8. Schematic diagram of the flow loop.

Table 2
Experimental operating conditions.

q_v (mL/min)	*Re*			
	MMC-1	MMC-SOC-1	MMC-2	MMC-SOC-2
211	329	321	283	278
264	411	401	354	348
316	494	482	425	417
369	576	562	495	487
422	658	642	566	556
475	740	723	637	626
527	823	803	708	695
580	905	883	778	765

The heat fluxes applied to the test chip range from 20 W/cm^2 to 35 W/cm^2 and eight mass flow rates: 20, 25, 30, 35, 40, 45, 50 and 55 kg/h are given to evaluate the test chip performance. The volume flow rates and corresponding Reynolds numbers tested in this work are presented in Table 2.

3.3. Measurement uncertainty

Different variables and the corresponding uncertainties are listed in Table 3. In terms of all measured variables, the instruments' uncertainties were provided by manufacturers. For those calculated parameters, an uncertainty analysis was performed using the method introduced in Ref. [54]. The calculated maximum uncertainties in Darcy friction factor f and total thermal resistance R_t are ±8.02% and ±2.54%, respectively.

Table 3
Variables and corresponding uncertainties.

Variables	Instrument	Accuracy
Mass flow rate	Coriolis mass flow meter	±0.2%
Inlet pressure	Gage pressure transducer	0.065%
Pressure drop	Differential pressure transducer	0.065%
Fluid temperature	T-type thermocouple	±0.1 °C
Chip temperature	RTDs	±0.23 °C
Keysight, N5752A	Heater voltage	±600 mV
	Heater current	±3.9 mA

3.4. Data reduction

Our numerical results [53] have demonstrated that larger convective heat transfer area would not necessarily bring lower thermal resistance and there's no need to consider the size of the convective heat transfer area when analyzing the performance of a microchannel heat sink. As for microchannel heat sink, the key purpose is to ensure the electronic work at reasonable temperature with the lowest pumping power. The pumping power is the product of the volume flow rate q_v and the pressure drop ΔP, so the pressure drop ΔP can represent the pumping power. Therefore, the pressure drop ΔP and the maximum total thermal resistance R_t are two essential parameters which can be used to characterize the performance of a microchannel heat sink.

The Reynolds number *Re* is calculated according to the density ρ and dynamic viscosity μ of the coolant:

$$Re = \frac{\rho u_{ave} D_h}{\mu}, \tag{2}$$

where u_{ave} is the average velocity of the liquid and D_h is the channel hydraulic diameter.

The Darcy friction factor f is used to measure the flow energy loss. For rectangular channel, it can be calculated by:

$$f = \frac{2\Delta P D_h}{L\rho u_{ave}^2}, \tag{3}$$

where ΔP is the pressure loss between the inlet and outlet of the test module and L is the flow length.

The maximum total thermal resistance R_t is an efficient index for evaluating the heat sink performance. R_t is conservatively calculated by the use of the temperature difference between the measured maximum chip temperature T_{max} and the measured inlet temperature T_{in}:

$$R_t = \frac{\Delta T_{max}}{Q} = \frac{T_{max} - T_{in}}{Q}, \tag{4}$$

where Q is the input power applied to the heater by a DC power supply and is the product of the voltage U and current I obtained from the power supply. It should be noted that the total thermal resistance consists of three parts: the conduction resistance of silicon, convection resistance and thermal resistance caused by the coolant temperature rise. The heat flux applied to the 1 × 1 cm^2

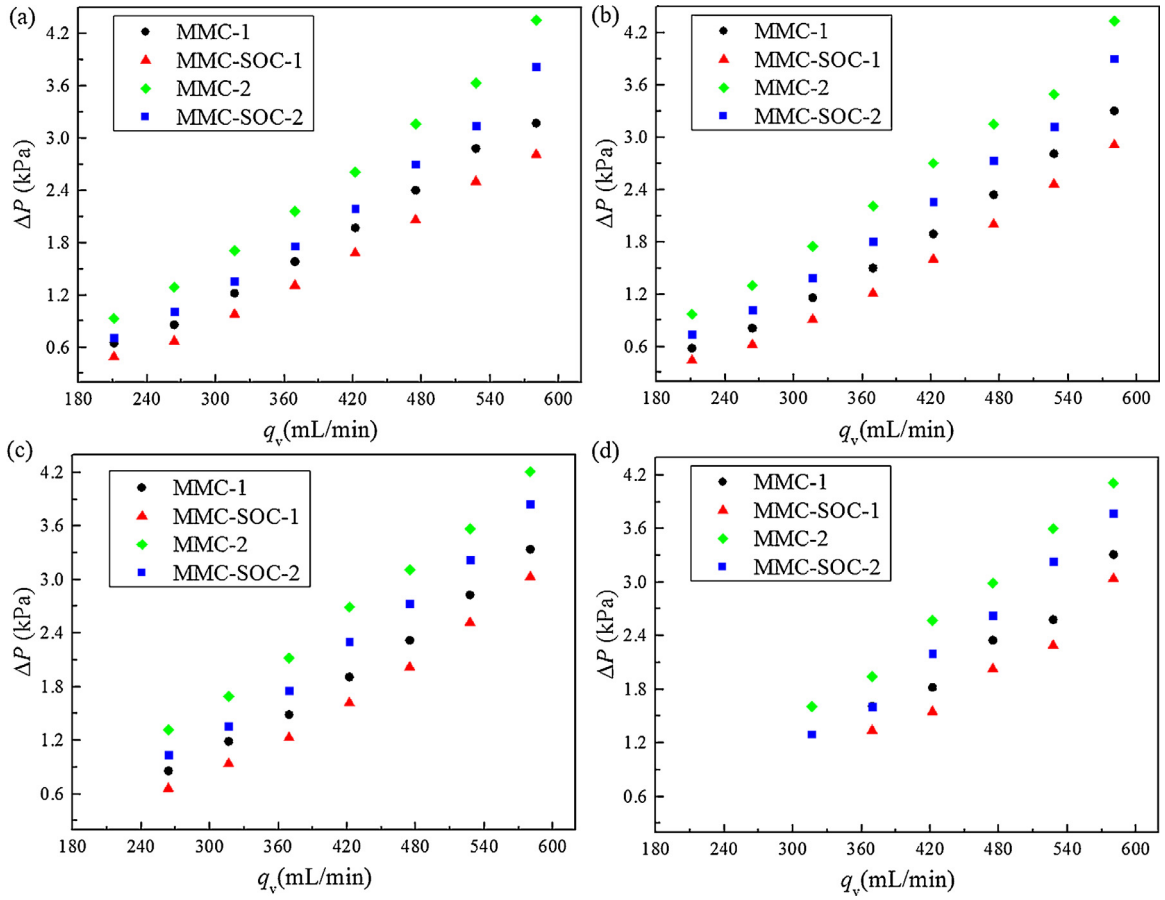

Fig. 9. Comparisons of pressure drop ΔP between MMC and MMC-SOC heat sinks at different volume flow rates for: (a) q''=20 W/cm^2, (b) q''=25 W/cm^2, (c) q''=30 W/cm^2 and (d) q''=35 W/cm^2.

heating area is then calculated as the quotient of the input power divided by the heating area.

4. Results and discussion

4.1. Hydrodynamic performance

Fig. 9 shows the experimental comparisons of pressure drop ΔP between MMC and MMC-SOC heat sinks at different volume flow rates (211–580 mL/min) and heat fluxes (20–35 W/cm^2). It can be seen that ΔP will increase with increasing volume flow rate q_v for MMC and MMC-SOC heat sinks, which agrees with the existing knowledge. It is important to note that the MMC-SOC heat sink has a lower pressure drop compared to MMC heat sink. As pointed out in our previous work [53], a dual effect of secondary channel on ΔP was observed. On the one hand, it can increase ΔP by promoting fluid mixing. On the other hand, it can reduce ΔP by providing more flow area. Moreover, the pressure drop reduction could be obtained if the structure is designed reasonably or the Reynolds number is small enough. Therefore, as can be seen from Fig. 9, the optimized MMC-SOC heat sink has a better hydraulic performance, i.e. lower pressure drop, compared to MMC heat sink at the current working conditions. The results are also described in a dimensionless form to provide a visual comparison between the hybrid heat sink and conventional manifold heat sink, as shown in Fig. 10. Here, the subscript 0 represents the performance of the conventional MMC heat sink. It is clear that the values of $(\Delta P/\Delta P_0)$ are all smaller than 1 under the working conditions, indicating that the proposed MMC-SOC heat sink has superior hydraulic performance compared to the conventional manifold

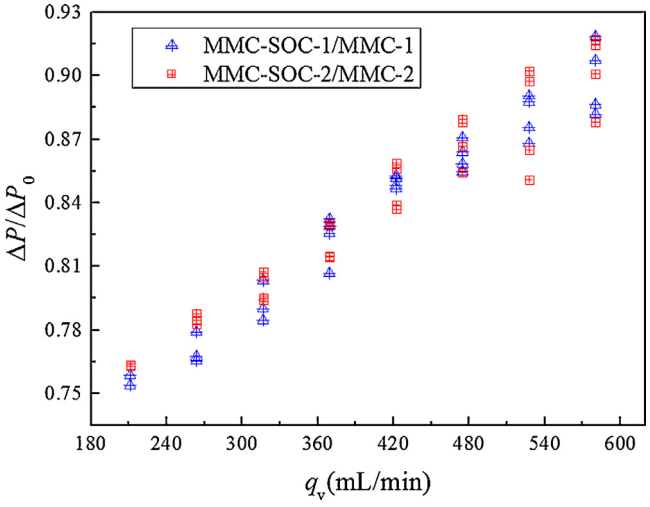

Fig. 10. Effects of volume flow rate q_v on the pressure drop ratio $(\Delta P/\Delta P_0)$.

microchannel heat sink. When the channel height H_c is 60 μm, the minimum value of pressure drop ratio $(\Delta P/\Delta P_0)$ is 0.75, and the maximum value is 0.92; for heat sinks with H_c=100 μm, the minimum value of $(\Delta P/\Delta P_0)$ is 0.76, and the maximum value is 0.97, indicating that the channel height has little effect on the value of $(\Delta P/\Delta P_0)$ in our study, while the flow rate is the main contributing factor. In addition, the secondary flow field analyses conducted in out previous work [53] have shown that a larger volume

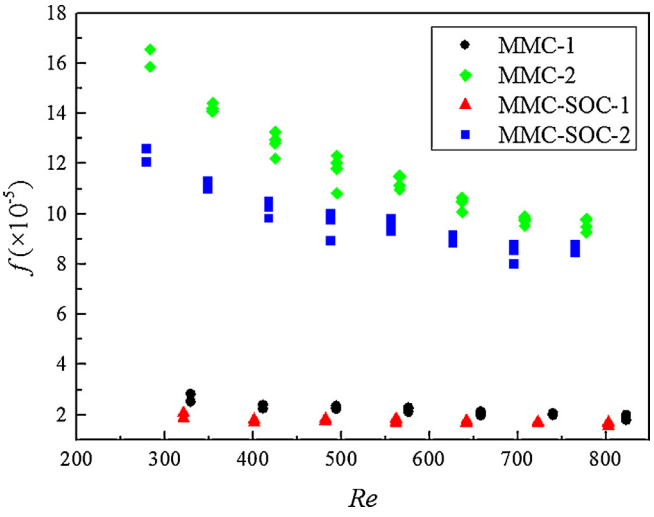

Fig. 11. The friction factor f as a function of the Reynolds number Re for all the four heat sinks.

flow rate q_v yields an improved fluid mixing and higher pressure loss penalty, which will increase the pressure loss ratio $(\Delta P/\Delta P_0)$. Fortunately, the values of $(\Delta P/\Delta P_0)$ are all less than 1 under the working conditions, even though the volume flow rate reaches up to 580 mL/min (the corresponding Reynolds number of the MMC-SOC heat sink reaches up to 883), demonstrating the dominate role of pressure drop reduction of secondary channel in this study. For example, for the maximum volume flow rate of 580 mL/min and a heat flux of 20 W/cm^2, the values of $(\Delta P/\Delta P_0)$ for heat sinks with H_c= 60 μm and H_c= 100 μm are 0.89 and 0.88, respectively. Lee et al. [48] carried out experimental study on the characteristics of secondary flow in microchannel and found that the secondary channel would lead to a significant increase in pressure loss when the Reynolds number exceeded 400 compared to straight microchannel. The foregoing analyses demonstrate an attractive feature of our hybrid design that it can reduce pressure loss at larger flow rates or Reynolds numbers. It should be noted that bubbles start to appear in the outlet tube when the flow rate is lower and the heat flux is higher, and those data points are removed from Figs. 9(c) and (d).

The experimental results of friction factor f of the four heat sinks under different heat fluxes are presented in Fig. 11. It is obvious that the friction factor f is influenced by many factors, such as Reynolds number, rib shape, channel size, etc. Whether for MMC or MMC-SOC heat sink, f will increase as the hydraulic diameter D_h of the channel increases, and decreases with increasing Reynolds number Re, which conforms to the existing knowledge. It should be pointed out that the friction factors of the MMC-1 and MMC-SOC-1 also have a clear dependence on Re if the scale range of the vertical coordinate becomes smaller. In addition, the MMC-SOC heat sink has smaller friction factor than the MMC heat sink with the same hydraulic diameter, indicating less flow energy consumption and a better hydraulic performance.

4.2. Thermal performance

Fig. 12 gives comparisons of the total thermal resistance R_t between MMC and MMC-SOC heat sinks under diffenent heat fluxes of 20–35 W/cm^2 and various volume flow rates of 211–580 mL/min. It is obvious that R_t decreases with increasing volume flow rate q_v for MMC and MMC-SOC heat sinks. The results are also described in a dimensionless form to provide a visual comparison, as shown in Fig. 13. It can be seen that the values of (R_t/R_{t0}) are all less than 1 under the working conditions, indicating a reduction in total thermal resistance of MMC heat sink. In addition, a larger q_v yields a smaller (R_t/R_{t0}) and a better thermal performance, which results from the improved fluid mixing and thinner boundary layer. The minimum value (R_t/R_{t0}) of heat sinks with H_c=60 μm is 0.76, which is obtained at the maximum flow rate (580 mL/min) and minimum heat flux (20 W/cm^2). The minimum value indicates that a 24% reduction in R_t can be observed compared to the conventional MMC heat sink under the same working condition. In addition, the thermal resistance ratio of heat sink with H_c= 60 μm is smaller than that with H_c = 100 μm under the same working condition. For example, the (R_t/R_{t0}) values of heat sink with H_c = 60 μm are 0.84, 0.79 and 0.75 at flow rates of 211, 316 and 580 mL/ min, respectively. However, those corresponding (R_t/R_{t0}) values of heat sink with H_c= 100 μm are 0.93, 0.90 and 0.84. It is observed that the value of (R_t/R_{t0}) will increase when increasing channel height H_c, demonstrating that a heat sink with higher channel height may have higher thermal resistance ratio. Higher H_c brings larger coolant flow area, which can decrease the flow velocity and Reynolds number. The numerical results [53] showed that lower flow velocity would bring weaker flow mixing in secondary channels, which could lead to a distinct inhibition in thermal performance enhancement. Therefore, heat sink with H_c= 60 μm has smaller value of (R_t/R_{t0}). In addition, the thermal resistance ratio is also related to the applied heat flux, which will be introduced in the next section. As mentioned above, some data points are removed from Figs. 12(c) and (d) due to the appearance of bubbles.

4.3. Overall performance

As pointed out by our early work [53], an effective cooling technique should maintain the temperature of various electronic devices within a reasonable range using the minimum cooling power. The pressure drop ΔP and the total thermal resistance R_t are two critical issues which should be considered. Therefore, the dependence of the dimensionless $(\Delta P/\Delta P_0)$ on (R_t/R_{t0}) for heat sinks with H_c= 60 μm and 100 μm are presented in Figs. 14 and 15, respectively. As shown in Figs. 14 and 15, a shadow area is plotted to illustrate the advantages of the hybrid MMC-SOC heat sink, i.e. the Design Optimization Area (DOA). In DOA, the values of (R_t/R_{t0}) and $(\Delta P/\Delta P_0)$ are both smaller than 1.

All of the data points are located in DOA, indicating that the proposed hybrid design with secondary channels can simultaneously reduce total thermal resistance R_t and pressure loss ΔP for all cases compared to the conventional MMC heat sink. For example, for the data shown in Fig. 14, the $(\Delta P/\Delta P_0)$ and (R_t/R_{t0}) values of heat sink with H_c = 60 μm are 0.89 and 0.76 for a volume flow rate of 580 mL/min and a heat flux of 20 W/cm^2, demostrating an 11% reduction in ΔP and a 24% reduction in R_t. For the data shown in Fig. 15, the $(\Delta P/\Delta P_0)$ and (R_t/R_{t0}) values of heat sink with H_c= 100 μm are 0.88 and 0.84, demostrating a 12% reduction in ΔP and a 16% reduction in R_t. It should be pointed out that the MMC-SOC heat sink can further reduce the thermal resistance compared to the MMC heat sink at the same pumping power. Increasing volume flow rate q_v will bring smaller (R_t/R_{t0}) and larger $(\Delta P/\Delta P_0)$, demonstrating an enhanced ability of reducing the maximum temperature and a suppressed ability of reducing the pressure drop. A larger q_v yields an improved fluid mixing and brings higher pressure loss penalty, which results in a reduction in (R_t/R_{t0}) and an increase in $(\Delta P/\Delta P_0)$. For the maximum q_v = 580 mL/min and q'' = 35 W/cm^2, the MMC-SOC-2 heat sink can maintain a maximum chip temperature of 53 °C with a pressure drop of only 3.77 kPa. The above trend indicates that the key advantage of the MMC-SOC heat sink over traditional MMC heat sink at larger flow rates is that it can reduce the chip temperature and thermal resistance significantly.

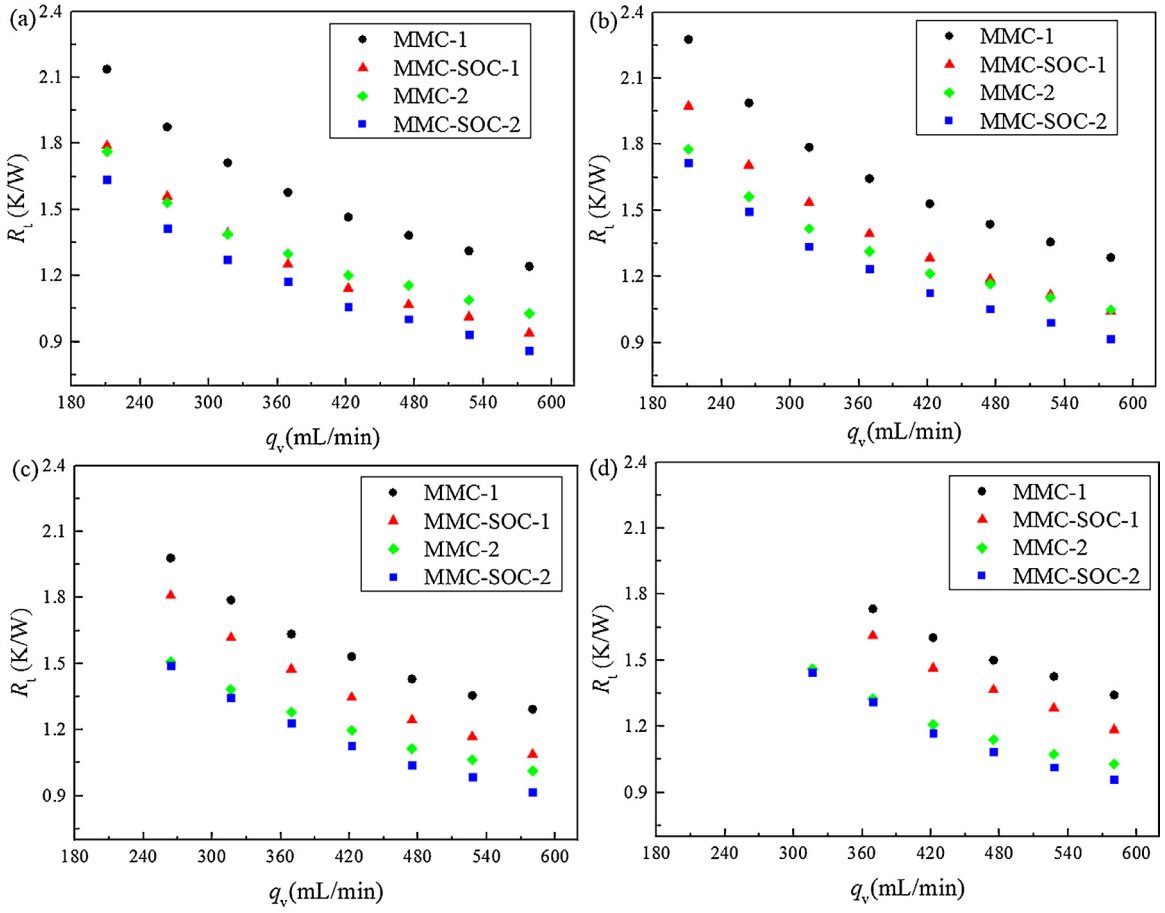

Fig. 12. Comparisons of total thermal resistance R_t between MMC and MMC-SOC heat sinks at different volume flow rates for: (a) q''=20 W/cm^2, (b) q''=25 W/cm^2, (c) q''=30 W/cm^2 and (d) q''=35 W/cm^2.

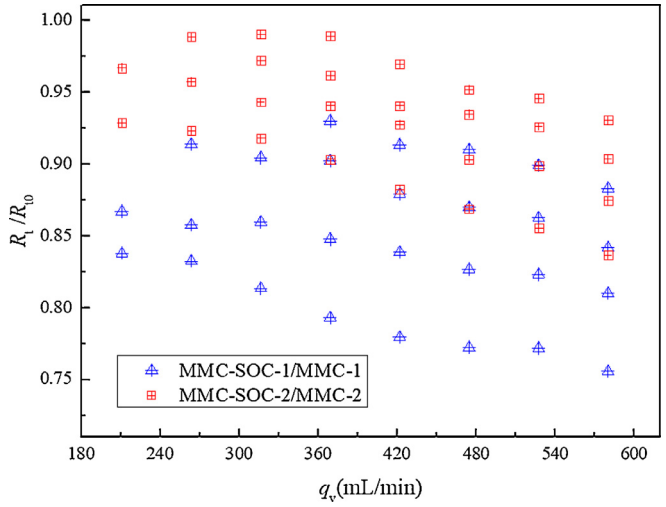

Fig. 13. Variation of thermal resistance ratio (R_t/R_{t0}) with volume flow rate q_v.

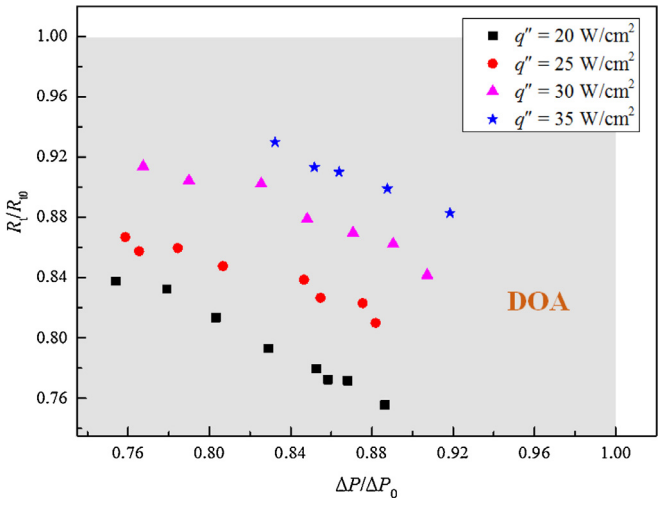

Fig. 14. Variation of thermal resistance ratio (R_t/R_{t0}) with pressure drop ratio ($\Delta P/\Delta P_0$) for heat sink with H_c= 60 μm.

Specific analyses show that there is no obvious systematic trend between the pressure drop ratio ($\Delta P/\Delta P_0$) and the variation of the heat flux, as can be seen form Figs. 14 and 15. The maximum fluid temperature difference between the inlet and outlet is less than 3 °C, which results in relatively constant thermo-physical properties. Certainly, the constant thermo-physical properties make the pressure drop ratio have nothing to do with heat flux. Furthermore, all data points will move up along the vertical axis as the heat flux increases, indicating an increase in the thermal resistance ratio (R_t/R_{t0}). This movement shows that the heat flux also has a suppression effect in the ability of MMC-SOC to reduce the maximum temperature. Therefore, increasing the flow rate becomes an effective way to further reduce the chip temperature at a higher heat flux. As q'' increases, the temperatures of the chip surface and the interface between the coolant and solid wall will increase rapidly

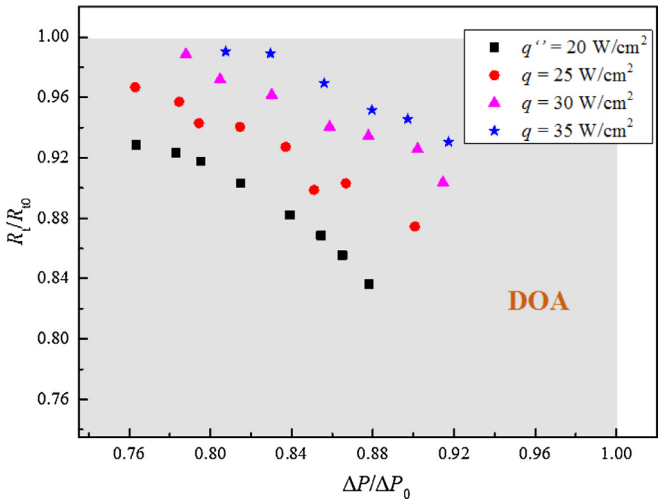

Fig. 15. Variation of thermal resistance ratio (R_t/R_{t0}) with pressure drop ratio ($\Delta P/\Delta P_0$) for heat sink with H_c= 100 μm.

due to the high thermal conductivity of silicon. A high temperature difference between the coolant and solid wall means that the heat can be transferred to the liquid quickly, no matter what the microchannel structure is. Therefore, the temperature difference severs as the dominant role in heat transfer process with high heat flux rather than the microchannel structure, which leads to an increase in (R_t/R_{t0}). However, it should be noted that the value of (R_t/R_{t0}) is influenced by multiple factors, including coolant types, further study should be carried out, which has beyond the scope of this paper.

5. Conclusions

In this work, the comparative studies between a hybrid microchannel heat sink and a conventional manifold mirochannel heat sink are carried out. The test chip containing heater, temperature sensors and microchannels is fabricated by lithography process and sputtering technique using a double-polished wafer. A 3D-printed manifold structure is used for chip packaging and flow guiding. The key conclusions are as follows:

(1) The fabricated hybrid heat sink has a DOA compared to the conventional manifold heat sink, indicating a simultaneous reduction in R_t and ΔP. The experimental results show that for channel height H_c= 60 μm, an 11% reduction in ΔP and a 24% reduction in R_t are observed for a volume flow rate of 580 mL/min and a heat flux of 20 W/cm^2;

(2) Increasing q_v will bring smaller total thermal resistance ratio (R_t/R_{t0}) and larger pressure drop ratio ($\Delta P/\Delta P_0$), indicating an enhanced ability of reducing the maximum temperature and a suppressed ability of reducing the pressure loss. A larger volume flow rate can result in improved fluid mixing and thinner boundary layer, which leads to a smaller (R_t/R_{t0}) and a larger ($\Delta P/\Delta P_0$). For the maximum q_v = 580 mL/min and q'' = 35 W/cm^2, the MMC-SOC-2 heat sink can maintain a maximum chip temperature of 53 °C with a pressure drop of only 3.77 kPa;

(3) Although the pressure drop penalties are higher for higher Reynolds numbers due to the enhanced fluid mixting, the proposed MMC-SOC heat sink has superior hydraulic performance compared to the conventional manifold microchannel heat sink owing to a reasonable design. For the maximum volume flow rate of 580 mL/min (the corresponding Reynolds number of the MMC-SOC heat sink reaches up to 883) and a heat flux of 20 W/cm^2, the values of ($\Delta P/\Delta P_0$) for heat sinks with H_c= 60 μm and H_c= 100 μm are 0.89 and 0.88, respectively. This provides a very promising scheme for safe and efficient operation of single-phase microchannel cooling;

(4) In addition, an increased (R_t/R_{t0}) is obtained when the heat flux increases. This trend may be caused by the dominant role of the temperature difference rather than the microchannel structure in heat transfer process with high heat flux. Therefore, increasing the flow rate becomes an effective way to further reduce the chip surface temperature at operating conditions with higher heat flux.

Declaration of Competing Interest

The authors declare that they have no known competing financial interests or personal relationships that could have appeared to influence the work reported in this paper.

CRediT authorship contribution statement

Min Yang: Conceptualization, Methodology, Formal analysis, Investigation, Data curation, Visualization, Writing - original draft, Writing - review & editing. **Mo-Tong Li:** Investigation, Visualization. **Yu-Chao Hua:** Formal analysis, Funding acquisition. **Wei Wang:** Writing - review & editing. **Bing-Yang Cao:** Supervision, Project administration, Funding acquisition.

Acknowledgement

This project is supported by the National Natural Science Foundation of China (Nos. 51825601, 51676108, 51906121), and the Initiative Postdocs Supporting Program of China Postdoctoral Science Foundation (No. BX20180155)

References

[1] G.E. Moore, Cramming more components onto integrated circuits, Electronics (Basel) 38 (1965) 114–117.
[2] M.M. Waldrop, The chips are down for Moore's law, Nat. News 530 (2016) 144–147.
[3] A.D. Franklin, Nanomaterials in transistors: from high-performance to thin-film applications, Science 349 (2015) 2750.
[4] K.N. Tu, Reliability challenges in 3D IC packaging technology, Microelectron. Reliab. 51 (2011) 517–523.
[5] Y. Pi, N. Wang, J. Chen, M. Miao, Y. Jin, W. Wang, Anisotropic equivalent thermal conductivity model for efficient and accurate full-chip-scale numerical simulation of 3D stacked IC, Int. J. Heat Mass Transf. 120 (2018) 361–378.
[6] S. Li, H. Zhang, J. Cheng, X. Li, W. Cai, Z. Li, F. Li, A state-of-the-art overview on the developing trend of heat transfer enhancement by single-phase flow at micro scale, Int. J. Heat Mass Transf. 143 (2019) 118476.
[7] F. Pourfattah, A.A.A. Arani, M.R. Babaie, H.M. Nguyen, A. Asadi, On the thermal characteristics of a manifold microchannel heat sink subjected to nanofluid using two-phase flow simulation, Int. J. Heat Mass Transf. 143 (2019) 118518.
[8] Z. Li, Y. Haramura, D. Tang, C. Guo, Analysis on the heat transfer characteristics of a micro-channel type porous-sheets Stirling regenerator, Int. J. Therm. Sci. 94 (2015) 37–49.
[9] Z. Yan, X. Huang, C. Yang, Hydrodynamic effects on particle deposition in microchannel flows at elevated temperatures, J. Heat Transf. (2018) 140.
[10] H.L. Li, Y.C. Hua, B.Y. Cao, A hybrid phonon Monte Carlo-diffusion method for ballistic-diffusive heat conduction in nano-and micro-structures, Int. J. Heat Mass Transf. 127 (2018) 1014–1022.
[11] F. Pourfattah, M. Sabzpooshani, Thermal management of a power electronic module employing a novel multi-micro nozzle liquid-based cooling system: a numerical study, Int. J. Heat Mass Transf. 147 (2020) 118928.
[12] W. Gao, X. Xu, X. Liang, Experimental study on the effect of orientation on flow boiling using R134a in a mini-channel evaporator, Appl. Therm. Eng. 121 (2017) 963–973.
[13] X.D. Zhang, X.P. Li, Y.X. Zhou, Y. Jiang, J. Liu, Vascularized liquid metal cooling for thermal management of kW high power laser diode array, Appl. Therm. Eng. 162 (2019) 114212.
[14] S.L. Wang, X.Y. Li, X.D. Wang, G. Lu, Flow and heat transfer characteristics in double-layered microchannel heat sinks with porous fins, Int. Commun. Heat Mass Transf. 93 (2018) 41–47.
[15] M. Yang, B.Y. Cao, W. Wang, H.M. Yun, B.M. Chen, Experimental study on capillary filling in nanochannels, Chem. Phys. Lett. 662 (2016) 137–140.

[16] X.L. Xie, Z.J. Liu, Y.L. He, W.Q. Tao, Numerical study of laminar heat transfer and pressure drop characteristics in a water-cooled minichannel heat sink, Appl. Therm. Eng. 29 (2009) 64–74.
[17] X. Luo, S. Liu, A microjet array cooling system for thermal management of high-brightness LEDs, IEEE Trans. Adv. Packaging 30 (2007) 475–484.
[18] R. Wu, Y. Fan, T. Hong, H. Zou, R. Hu, X. Luo, An immersed jet array impingement cooling device with distributed returns for direct body liquid cooling of high power electronics, Appl. Therm. Eng. 162 (2019) 114259.
[19] S. Wiriyasart, P. Naphon, Liquid impingement cooling of cold plate heat sink with different fin configurations: high heat flux applications, Int. J. Heat Mass Transf. 140 (2019) 281–292.
[20] X. Zhao, Z. Yin, B. Zhang, Z. Yang, Experimental investigation of surface temperature non-uniformity in spray cooling, Int. J. Heat Mass Transf. 146 (2020) 118819.
[21] L.J. Jiang, S.L. Jiang, W.L. Cheng, Y.L. Nian, R. Zhao, Experimental study on heat transfer performance of a novel compact spray cooling module, Appl. Therm. Eng. 154 (2019) 150–156.
[22] N. Liu, Z. Yu, Y. Liang, H. Zhang, Effects of mixed surfactants on heat transfer performance of pulsed spray cooling, Int. J. Heat Mass Transf. 144 (2019) 118593.
[23] D.B. Tuckerman, R.F.W. Pease, High-Performance Heat Sinking for VLSI, IEEE Electron Device Lett EDL-2 (1981) 126–129.
[24] G. Wang, N. Qian, G. Ding, Heat transfer enhancement in microchannel heat sink with bidirectional rib, Int. J. Heat Mass Transf. 136 (2019) 597–609.
[25] A. Moradikazerouni, M. Afrand, J. Alsarraf, O. Mahian, S. Wongwises, M.D. Tran, Comparison of the effect of five different entrance channel shapes of a micro-channel heat sink in forced convection with application to cooling a supercomputer circuit board, Appl. Therm. Eng. 150 (2019) 1078–1089.
[26] P. Li, D. Guo, X. Huang, Heat transfer enhancement in microchannel heat sinks with dual split-cylinder and its intelligent algorithm based fast optimization, Appl. Therm. Eng. (2020) 115060.
[27] M.A. Alfellag, H.E. Ahmed, A.S. Kherbeet, Numerical simulation of hydrothermal performance of minichannel heat sink using inclined slotted plate-fins and triangular pins, Appl. Therm. Eng. 164 (2020) 114509.
[28] A.G. Fedorov, R. Viskanta, Three-dimensional conjugate heat transfer in the microchannel heat sink for electronic packaging, Int. J. Heat Mass Transf. 43 (2000) 399–415.
[29] C.Y. Zhao, T.J. Lu, Analysis of microchannel heat sinks for electronics cooling, Int. J. Heat Mass Transf. 45 (2002) 4857–4869.
[30] S.J. Kim, D. Kim, D.Y. Lee, On the local thermal equilibrium in microchannel heat sinks, Int. J. Heat Mass Transf. 43 (2000) 1735–1748.
[31] W. Qu, I. Mudawar, Experimental and numerical study of pressure drop and heat transfer in a single-phase micro-channel heat sink, Int. J. Heat Mass Transf. 45 (2002) 2549–2565.
[32] L. Liang, J. Hou, X. Fang, Y. Han, J. Song, L. Wang, Z. Deng, G. Xu, H. Wu, Flow characteristics and heat transfer performance in a Y-Fractal mini/microchannel heat sink, Case Stud. Therm. Eng. 15 (2019) 100522.
[33] Y. Chen, F. Yao, X. Huang, Mass transfer and reaction in methanol steam reforming reactor with fractal tree-like microchannel network, Int. J. Heat Mass Transf. 87 (2015) 279–283.
[34] Y. Sui, C.J. Teo, P.S. Lee, Y.T. Chew, C. Shu, Fluid flow and heat transfer in wavy microchannels, Int. J. Heat Mass Transf. 53 (2010) 2760–2772.
[35] H.A. Mohammed, P. Gunnasegaran, N.H. Shuaib, Numerical simulation of heat transfer enhancement in wavy microchannel heat sink, Int. Commun. Heat Mass Transf. 38 (2011) 63–68.
[36] F. Zhou, W. Zhou, Q. Qiu, W. Yu, X. Chu, Investigation of fluid flow and heat transfer characteristics of parallel flow double-layer microchannel heat exchanger, Appl. Therm. Eng. 137 (2018) 616–631.
[37] C. Leng, X.D. Wang, T.H. Wang, W.M. Yan, Multi-parameter optimization of flow and heat transfer for a novel double-layered microchannel heat sink, Int. J. Heat Mass Transf. 84 (2015) 359–369.
[38] H. Shen, G. Xie, C.C. Wang, The numerical simulation with staggered alternation locations and multi-flow directions on the thermal performance of double-layer microchannel heat sinks, Appl. Therm. Eng. 163 (2019) 114332.
[39] G.M. Harpole, J.E. Eninger, Micro-channel heat exchanger optimization, in: 7th IEEE SEMI-THERM Symposium, 1991, pp. 59–63.
[40] M. Pan, X. Zhong, G. Dong, P. Huang, Experimental study of the heat dissipation of battery with a manifold micro-channel heat sink, Appl. Therm. Eng. 163 (2019) 114330.
[41] Y. Luo, J. Li, K. Zhou, J. Zhang, W. Li, A numerical study of subcooled flow boiling in a manifold microchannel heat sink with varying inlet-to-outlet width ratio, Int. J. Heat Mass Transf. 139 (2019) 554–563.
[42] S. Wang, H.H. Chen, C.L. Chen, Enhanced flow boiling in silicon nanowire–coated manifold microchannels, Appl. Therm. Eng. 148 (2019) 1043–1057.
[43] D. Kong, K.W. Jung, S. Jung, D. Jung, J. Schaadt, M. Iyengar, C. Malone, C.R. Kharangate, M. Asheghi, K.E. Goodson, H. Lee, Single-phase thermal and hydraulic performance of embedded silicon micro-pin fin heat sinks using R245fa, Int. J. Heat Mass Transf. 141 (2019) 145–155.
[44] K.P. Drummond, D. Back, M.D. Sinanis, D.B. Janes, D. Peroulis, J.A. Weibel, S.V. Garimella, A hierarchical manifold microchannel heat sink array for high-heat-flux two-phase cooling of electronics, Int. J. Heat Mass Transf. 117 (2018) 319–330.
[45] S. Wang, H.H. Chen, C.L. Chen, Enhanced flow boiling in silicon nanowire–coated manifold microchannels, Appl. Therm. Eng. 148 (2019) 1043–1057.
[46] K.P. Drummond, J.A. Weibel, S.V. Garimella, Two-phase flow morphology and local wall temperatures in high-aspect-ratio manifold microchannels, Int. J. Heat Mass Transf. 153 (2020) 119551.
[47] G. Xia, Y. Lv, D. Ma, Y. Jia, Experimental investigation of the continuous two-phase instable boiling in microchannels with triangular corrugations and prediction for instable boundaries, Appl. Therm. Eng. 162 (2019) 114251.
[48] Y.J. Lee, P.S. Lee, S.K. Chou, Enhanced microchannel heat sinks using oblique fins, ASME 2009 InterPack Conf. 2 (2009) 253–260.
[49] N.R. Kuppusamy, R. Saidur, N.N.N. Ghazali, H.A. Mohammed, Numerical study of thermal enhancement in micro channel heat sink with secondary flow, Int. J. Heat Mass Transf. 78 (2014) 216–223.
[50] L. Chai, L. Wang, X. Bai, Thermohydraulic performance of microchannel heat sinks with triangular ribs on sidewalls–Part 2: average fluid flow and heat transfer characteristics, Int. J. Heat Mass Transf. 128 (2019) 634–648.
[51] Z.Y. Guo, D.Y. Li, B.X. Wang, A novel concept for convective heat transfer enhancement, Int. J. Heat Mass Transf. 41 (1998) 2221–2225.
[52] Q. Yang, J. Zhao, Y. Huang, X. Zhu, W. Fu, C. Li, J. Miao, A diamond made microchannel heat sink for high-density heat flux dissipation, Appl. Therm. Eng. 158 (2019) 113804.
[53] M. Yang, B.Y. Cao, Numerical study on flow and heat transfer of a hybrid microchannel cooling scheme using manifold arrangement and secondary channels, Appl. Therm. Eng. 159 (2019) 113896.
[54] R.J. Moffat, Describing the uncertainties in experimental results, Exp. Therm. Fluid Sci. 1 (1988) 3–17.